RECEIVED BY OSTI JUL 05 1985

CONF-850736--9

LA-UR 85-2287

TITLE COMPARATIVE RESPONSE OF ALLUVIUM TO HOPKINSON BAR AND GAS GUN LOADING

LA-UR--85-2287

DE85 014068

AUTHOR(S) E. S. Gaffney (ESS-5)
J. A. Brown (ESS-3)

SUBMITTED TO 1985 APS Topical Conference on Shock Waves in Condensed Media, July 22-25, 1985, Spokane, WA

COMPARATIVE RESPONSE OF ALLUVIUM TO HOPKINSON BAR AND GAS GUN LOADING

E. S. Gaffney and J. A. Brown

Earth and Space Sciences Division
Los Alamos National Laboratory
Los Alamos, NM 87545

INTRODUCTION

Low amplitude shock waves in highly dispersive media such as dry alluvium quickly degenerate into ramp waves. One result of this behavior is that standard explosive techniques used for dynamic testing of such materials do not produce data under conditions relevant to most real applications such as confinement of buried explosions or assessment of the effects of explosions on buried structures. We have developed techniques for testing soils dynamically at strain rates ranging from about 10^2 to about 10^4 sec^{-1} in uniaxial strain using a Hopkinson bar. This admits direct comparison with data from gas gun tests where strain rates are in the range of 10^4 to 10^5 sec^{-1}. This, in turn, permits the separation of inertial effects from direct strain-rate effects. In order to assist in evaluation of the results we have also developed a one dimensional microphysical model of soil.

EXPERIMENTAL METHODS

A Hopkinson bar is shown schematically in Figure 1. It consists essentially of two long, round bars. A cylindrical specimen is placed between the two bars and a compressive stress pulse is generated at the far end of one of the bars. This pulse travels the length of the bar where it is incident on the sample (hence the term incident bar). At the interface between the incident bar and the specimen, part of the energy is reflected back into the incident bar as a reflected pulse and part is transmitted into the specimen. This latter continues through the specimen to the other surface where a portion of it continues into the other bar (called the transmitter bar) as a transmitted pulse. The stress pulses in the bars are recorded with strain gauges mounted sufficiently distant from either end to prevent overlap of the wavetrains. A momentum trap at the end of the transmitter bar prevents multiple reflections of the transmitted stress wave. The bars remain elastic during the passage of the stress wave so the strain gauges accurately reproduce the stress histories in the bars.

Our Hopkinson bar consists of incident and transmitter bars supported by a reaction frame. The bars are 60.3 mm diameter, 1.22 m long, maraging steel with a yield stress of about 2 GPa. Teflon bushings in the cross members of the reaction frame support the bars at about half meter intervals. Stress waves in the bars are monitored by strain gauge pairs

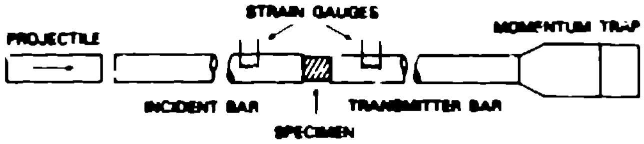

Figure 1. Schematic of Hopkinson bar apparatus.

mounted 0.61 m from the specimen ends. The pairs are used in half bridge configuration to null bending strains. The incident stress pulse is generated by impact of a projectile from a small gas gun. Projectile velocity is measured just prior to impact by three pairs of diode lasers and photodetectors mounted in the muzzle of the gun.

The soil studied was alluvium from near Yuma, AZ. The water content was 3.5 percent of dry weight, and the initial bulk density was 1770 kg/m^3. It was necessary to provide radial support merely to keep the specimen in position for the test. We have used a thick-walled cylinder of bronze or steel with an axial hole just slightly larger than the diameter of the bar, as shown in Figure 2. This very stiff support has the advantages of being easy to implement and providing a strain path that can be duplicated at higher and lower strain rates - uniaxial strain. This strain path also facilitates data analysis, as we shall show below. Tests with no samples have shown that the sleeve carries substantially less than 0.1 percent of the stress pulse during loading. Radial strains in this configuration are less than 0.01 percent while there is still substantial gas-filled porosity remaining in the soil.

The gas gun used in these tests has a 200 mm bore and is capable of firing a 6.5 kg projectile at velocities up to 350 m/sec. The gas gun target is illustrated in Figure 3. The sample was compacted in three lifts 183 mm in diameter and 12.7 mm thick with two embedded piezoresistive carbon stress gauges. The sample was encapsulated in plexiglas. Pins to measure the projectile velocity were secured in the plexiglas rings surrounding the radial surface of the target. The plexiglas also contained embedded carbon gauges to measure the stress delivered to the sample and transmitted through it. The gauges in the plexiglas were separated from the sample by 1.3 to 1.6 mm. In-material gauge packages were made by encapsulating the carbon gauge (with 13 μm of Kapton on each side of the gauge element) in 0.38 mm of electronic grade mica sheet on each side, providing heavy leads (#20 copper) through the plexiglas and wedges of plexiglas (as shown in Figure 2) to spread the shear caused by the transition from soil to plexiglas.

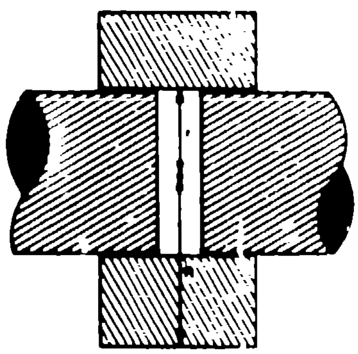

Figure 2. Hopkinson bar sample holder for soil.

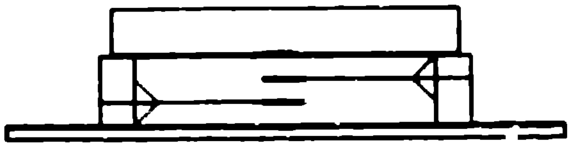

Figure 3. Gas gun target.

Both types of data were recorded by multichannel CAMAC-based waveform digitisers (IEEE-583 Std.), with 8-bit resolution. Sampling rates were 2 MHz for the Hopkinson bar and 4 MHz for the gun. In both cases the analog bandwidth of the recording system was about 1 MHz. The recorded data were automatically read by a small microcomputer and stored on flexible disk for later processing on a larger machine.

ANALYTICAL METHODS

Raw data from both the gas gun experiments and the Hopkinson bar tests were in the form of stress histories - at Lagrangian locations for the former and at the interfaces between the bars and the samples for the latter. We have converted both types of data to stress-strain paths using the Lagrangian analysis algorithms of Seaman [1]. Since the gas gun data is indeed Lagrangian, their treatment is straightforward and will not be discussed further. However, the treatment of the Hopkinson bar data will be described in some detail in the remainder of this section.

The strain pulses are shifted in time to coincide with the transit time to or from the center of the sample. We have used the method of Follansbee and Frantz [2] to correct for rod wave dispersion. This procedure also removes the high frequencies in the data which are noise.

The velocity measurement at the transmitted interface can not be considered to be a Lagrangian measurement in an unperturbed flow field. However, we have been able to convert the data to a Lagrangian, free-field equivalent using a technique which relies on observation of the change in wave speed between the first wave transmitted through the soil and the first wave reflected off the rear interface. It is usually possible to determine the velocity of these two waves from the data; we have sometimes detected the second reflection arriving at the transmitter bar.

Consider the experiment in pressure-particle velocity space as illustrated in figure 4. The stress wave in the bar loads the steel from the origin to the peak of the steel load-unload curves. When the wave encounters the interface, the steel unloads to the state designated u_f, P_f which is also the state in the soil. However, when that wave (or its attenuated counterpart) arrives at the rear of the sample, it encounters steel that is not moving, and a reflected state is measured which lies at the intersection of the reflected loading curve for the soil and the initial loading curve for the steel at u_m, P_m. If the speed of the reflected wave is n times that of the incident wave, we find that the ratios are

$$(u_f/u_m) = (\rho_b D_b/(n+1)\rho_s D_s) + n/(n+1)$$

and

$$(P_f/P_m) = n(\rho_s D_s/(n+1)\rho_b D_b) + 1/(n+1).$$

The technique just outlined will work well so long as the loading curve of the soil is fairly smooth and all waves are compressive. If the loading curve is not smooth, the reflection coefficients just derived will not be nearly constant, and a simple multiplicative factor will not relate the free-field and measured wave forms. This might occur if the soil has a

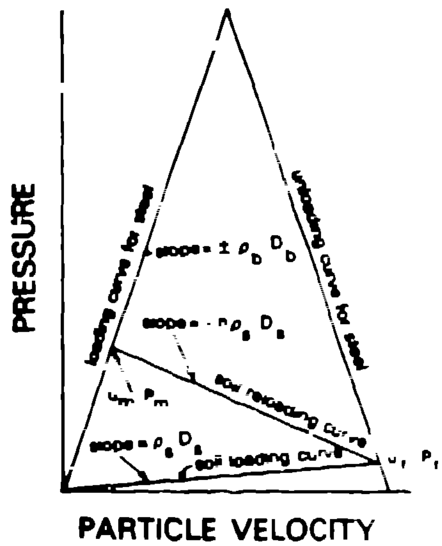

Figure 4. Hopkinson bar test of soil in pressure-particle velocity space.

very sharply defined yield point or when all the gas-filled porosity has been eliminated. In the former case, the reflection coefficient will decrease drastically as the yield point is exceeded, whereas in the latter case it will increase sharply. If the incident wave has a rarefaction phase, this will likely have a much higher speed than the wave which would occur upon its reflection from the transmitter bar. This would result in a very complicated geometric relation in the pressure-particle velocity plane. Although a scheme comparable to the one just described could probably be developed, this has not been accomplished to date. Consequently we treat only the initial loading portion of the experiments here.

To illustrate this method, consider the data from the four experiments shown in Figure 5. Two of the experiments used a sample 25 mm thick (22 and 24) and the other two used 13 mm samples. Experiments 21 and 22 used the same impactor and 23 and 24 used a second impactor. We have analysed both experiments with the same impactor as a single set, scaling the amplitude of the data from the 25 mm experiment up or down by the amount necessary to bring the incident pulses into coincidence. Incident wave amplitudes for each pair of experiments are within 2 percent of the same value. Data from experiments 21, 23 and 24 show that reflections off the transmitter bar travel about 1.6 times faster (Lagrangian wave speed) than those incident on that bar; a second reflection seen on experiment 24 shows a similar increase. Since the density is changing by only about 10 percent at the most, we have used $n = 1.6$ in our analysis. With the initial soil density of 1770 kg/m^3 and an incident wave speed of 220 m/s and the corresponding values for the bar (8100 kg/m^3 and 4860 m/s) we find that $u_f/u_m = 40.$ and $P_f/P_m = 0.39$. With this scale factor for the velocities at the transmitted interface, we can use Seaman's technique to calculate the free-field stress histories and find satisfactory agreement with the calculated stress ratio.

RESULTS AND DISCUSSION

The stress-strain paths observed in the gas gun experiment and the four Hopkinson bar experiments are shown in Figure 5 along with a quasistatic uniax. The strain rates in the Hopkinson bar tests reach 5000 s^{-1} and the strain accelerations reach about 2.5×10^{6} s^{-2}. The Hopkinson bar data are indistinguishable from the static loading. The gas gun data,

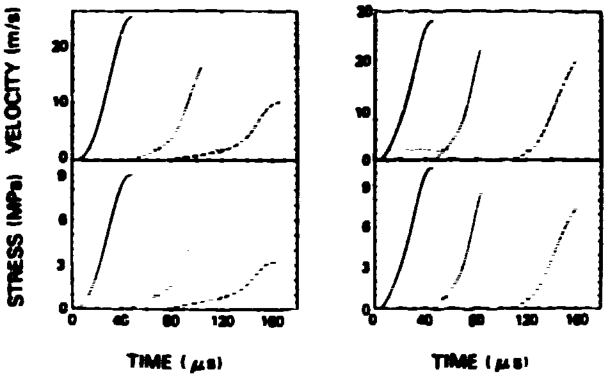

Figure 5. Velocity (upper) and stress (lower) histories measured at sample interfaces. (a) Tests 21 and 22. (b) Tests 23 and 24.

which represent strain rates up to 10^4 and 3×10^4 s^{-1} and accelerations up to 6×10^9 s^{-2}, lie substantially above the other curves. Because of the similarity of strain rates at the lower end of the gas gun regime and the upper end of the Hopkinson bar regime, the distinct behavior of the soil in the gas gun tests is probably due to inertial effects rather than to direct strain-rate effects.

The loading behavior of this soil can be reproduced by a simple one-dimensional soil model which treats the soil as a collection of cells, each composed of three elements. A typical cell consists of two rigid half cubes of a sand grain ℓ on a side separated by void and a pillar of a Bingham material of dimension $\ell\times\ell\times\ell\phi_c/(1-\phi_s)$, where ϕ_c and ϕ_s are the volume fractions of clay and sand, respectively. By considering the strength, "viscous" flow, and horizontal and vertical inertia of the deforming clay pillar, along with the inertia of the sand, the stress-strain relation for this cell can be written as

$$\sigma = \frac{\ell^2\phi_c\sigma_o}{(1-\phi_s-\epsilon)} + \frac{3\mu\phi_c^3\phi_s^2\dot{\epsilon}}{4(1-\phi_s-\epsilon)^6} + \frac{\phi_c\rho_c\ell^2}{2(1-\phi_s-\epsilon)^4}\left(\frac{\phi_c\ell_s\dot{\epsilon}^2}{(1-\phi_s-\epsilon)} + \frac{\ddot{\epsilon}}{2}\right) + \ell^2\left(\frac{\rho_s}{\phi_s} + \frac{\rho_c\phi_c}{\phi_s^2}\right)\ddot{\epsilon},$$

where ρ_s and ρ_c are the densities of the sand and clay, respectively, and σ_o is the strength and μ the "viscosity" of the Bingham material.

At first glance, this appears a rather fearsome formulation. However, of seven material properties in the expression (σ_o, μ, ϕ_c, ϕ_s, ρ_c, ρ_s and ℓ), only the first two cannot be determined by standard soil analysis methods. The value of ρ_s will be the grain density of the sand fraction of the soil. The value of ρ_c can be calculated from the grain density of the silt and clay fraction plus the water content. Values for ℓ, ϕ_c and ϕ_s will have distributions in a typical soil, but their mean values can be determined readily from the standard grain-size analysis. For the soil studied, the mean values of ϕ_s and ϕ_c are 0.57 and 0.15, respectively, and the mean grain size of the sand fraction was assumed to be 0.5 mm. The sand was predominantly quartz and feldspar, so we have taken ρ_s to be 2650 kg/m^3. We estimate ρ_c to be about 2400 kg/mo.

The low strain portion of the static behavior is most sensitive to the distribution of ϕ_c and to σ_o. We have assumed a beta-distribution for ϕ_c

$$P(\phi_c) = B(1.5,2.25)\left(\frac{\phi_c}{1-\phi_s}\right)^{0.5}\left(1-\frac{\phi_c}{1-\phi_s}\right)^{2.25},$$

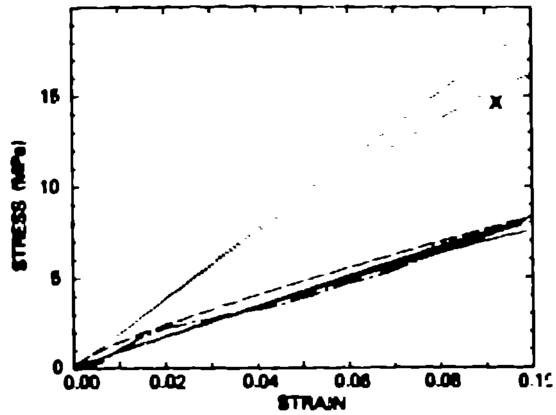

Figure 6. Stress-strain paths in dry alluvium: — - — static, —— Hopkinson bar, ······· gas gun, — — calculated static, x calculated gas gun.

where B is the beta function. With a yield stress of 10 MPa we get a static stress-strain curve as shown in Figure 6. With $\mu = 10^3$ Pa·s, neither the Hopkinson bar nor the gas gun response would be appreciably above the static curve in the absence of inertial effects. Although we have not yet calculated the complete loading path using the real strain histories, the inertial effects would bring the stress-strain path close to the measured gas gun response with the major inertial contribution being from the sand fraction. For example, the stress-strain point indicated by the symbol in Figure 6 would be predicted for the nominal strain, strain rate and strain acceleration of the gas gun tests.

In simulating the behavior of this soil we have merely selected σ_o and μ to fit the data. There is an extensive literature on the rheology of clay-water mixtures. For most such mixtures, the strength and "viscosity" used here would be high, but these properties are very sensitive to the solids:water ratio at high solid concentrations [4,5]. We have been unable to locate any data for mixtures as dry as the one considered, and extrapolation from four times our water contents can give values on the order of those used here. However, we have little confidence in the extrapolations.

This soil model is clearly very simplified and requires extensive further development before it could be considered predictive. Nevertheless, it does permit some evaluation of the relative importance of inertial effects and direct strain-rate effects in soil. The model supports our conclusion based solely on the data that the difference between the response of dry alluvium to testing in the gas gun and testing at lower rates is primarily attributable to inertial effects.

REFERENCES

[1] Seaman, L., Lagrangian analysis for multiple stress or velocity gauges in attenuating waves. J. Appl. Phys. 45, 4303-4310 (1974).
[2] Follansbee, P. S., and C. Frantz, Wave propagation in the split Hopkinson pressure bar. J. Eng. Mater. Tech. 105, 61-66 (1983).
[3] Gaffney, E. S., Preliminary constitutive model for alluvium. Los Alamos National Laboratory memo ESS-5:85-OU-410, June 1985.
[4] Norton, F. H., A. L. Johnson and W. G. Lawrence, Fundamental study of clay: VI, Flow properties of kaolinite-water suspensions. J. Amer. Ceram. Soc. 27, 149-164 (1944).
[5] Nguyen, Q. D., and D. V. Boger, Yield stress measurements for concentrated suspensions. J. Rheol. 27 321-349 (1983).